Computer Simulations of Short Exposure Images of A single and Binary Star

A. T. Mohammed and A. J. Tawfiq
Department of Astronomy, College of Science, University of Baghdad, Baghdad-Iraq.
Received:7/12/2005 Accepted: 17/4/2006

Abstract

The problem of atmospheric turbulence has taken a considerable amount of attentions in the literatures. Most of theise studies have not considering the quantitative aspects of the seeing conditions in terms of mathematical representation.
The study involves two-dimensional computer simulations of short exposure recording using Kolmogorov approach. The quality of these images is quantified in order to see the effects of atmospheric turbulence on the observed images. This assessment shows clearly the parameters that affect the possibilities of approaching diffraction limiting resolution of the telescope.
The results demonstrate that the average frequency components are linearly proportional to the square of the telescope radius and linearly proportional to the seeing conditions.
Signal to noise and signal to background ratios of the autocorrelation function of a binary star as a function of telescope diameter and seeing conditions are calculated.

الخلاصة

ان مشكلة التقلبات الجوية اخذت اهتماماً كبيراً في موضوع صور التلسكوبات وان معظم هذه الدراسات لم تأخذ بنظر الأعتبار المفاهيم الكمية لحالات الرؤيا في جدول التمثيل الرياضي.
ان هذه الدراسة تتضمن محاكاة ببعدين لصور التعرض القصير باستخدام تقريب Kologorov . ان نوعية الصور تمت دراستها بصورة كمية وذلك لرؤية التاشيرات الرقمية على نوعية هذه الصور.
الدراسة اثبتت ان معدل مركبات الترددات لهذه الصور تتناسب طردياً مع مربع نصف قطر التلسكوب وخطياً مع حالات الرؤيا. تم ايضاً دراسة نسبة الأشارة الى الضوضاء والأشارة الى الخلفية الأرضية لهذه الصور.

Introduction

All telescopes have an inherent limitation to their angular resolution due to the diffraction of light at the telescope's aperture.
The incoming light is approximately a plane wave since the source of the light is so far away. In this far field limit, Fraunhofer diffraction occurs and the pattern projected onto the focal plane of the telescope will have little resemblance to the aperture. According to Rayleigh criterion, and if $\lambda = 450$ nm , $D=6$ *m*, the resolving power is equal to $(0.0188\ 7'')$. In the presence of atmospheric turbulence, this resolution may becomes $1''$ or more.
Many observatories, including the Mount Wilson Observatory [1], European Southern Observatory [2] and [3], constantly monitor the local seeing conditions. These data can be used for setting observing schedules, assessing facility upgrade feasibility, and designing high resolution imaging instruments [4].

When imaging an object through the atmosphere, however, the wave front has passed through many

such turbulent layers, each characterized by different average densities and velocities. By observing centroid motion as a measure of the variation in angle of arrival, Fried [5] used the model of atmospheric turbulence developed by Kolmogorov [6] and Tatarski [7] to quantitatively relate the results to seeing.

Measurements of the space time correlation function of images at the focus of a large telescope have been studied by [8]. The results indicate that the image boiling has a directional component that is parallel to the motion of the turbulence in the pupil plane.

Techniques to overcome the effects of the atmosphere have been developing rapidly. These techniques can be grouped into two categories: pre-detection and post-detection. Welsh and Roggemann [9], using the post detection scene technique in order to deconvolve wave front sensing (DWFS). A wave front sensor (WFS) is used to record the wave front phase distortion in the pupil of the telescope for each short exposure image. The addition information provided by the WFS is used to estimate the system's *point spread function* (psf). The psf is then used in conjunction with the ensemble of short exposure images to obtain an estimate of the object intensity distribution via deconvolution.

The objective of this paper is to study quantitatively the effects of telescope apertures on the actual power spectra and the autocorrelation functions of short exposure images of a binary star in the presence of atmospheric turbulence using different size of telescope apertures.

Image Formation Model

When an optical system produces an image using perfectly incoherent light, then the function, which describes the intensity in the image plane produced by a point object plane, is called the Impulse Response Function. The input (object intensity pattern) and output (image intensity pattern) are related by the simple convolution.

Since it is impossible to construct a truly infinitesimal source, one cannot directly measure the response of a system to a point impulse. The following diagram represents the calculation of the OTF and MTF.

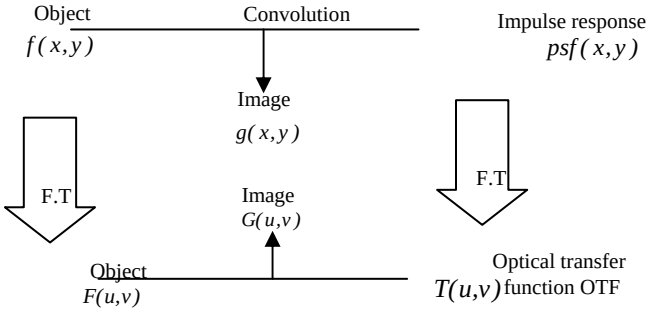

Fig. (1): ***Calculation of the optical transfer function in incoherent light***

It is important to study the effects of the telescope aperture on the actual psf and the modulation transfer function, MTF. The pupil function $H(\eta,\gamma)$ in the absence of atmospheric turbulence is given by:

$$H(\eta,\gamma)=\begin{cases}1 & if \quad \left[(\eta-\eta_c)^2+(\gamma-\gamma_c)^2\right]^{1/2} < R \\ 0 & otherewise\end{cases} \qquad (1)$$

where R is the radius of the telescope aperture.

The instantaneous psf of the telescope system alone is given by:

$$psf\ (x,y) = \left| FT\ [H(\eta,\gamma)] \right|^2 \qquad (2)$$

The MTF of a system may be measured by one of two methods: auto-correlating the pupil function of the lens-under-test or analyzing the psf calculated by Fourier transforming the pupil wave front. The transfer function of an incoherent optical system is equal to the autocorrelation of the pupil function [10],

$$T(u,v)=\int_{-\infty-\infty}^{+\infty+\infty} H(\eta',\gamma')H^{\bullet}(\eta+\eta',\gamma+\gamma')d\eta'd\gamma' \qquad (3)$$

The variables (η,γ) represent distances in the pupil, and are related to the spatial frequency variables (u,v) by:

$$\eta = f\lambda u; \qquad \gamma = f\lambda v \qquad (4)$$

where f is the focal length.

MTF is then computed by taking the absolute of Eq. (3).

Atmospheric Turbulence:

Large scale temperature inhomogeneities caused by differential heating of different portions of the Earth's surface produce random micro-structures in the spatial distribution of temperature which, in turn, cause the random fluctuations in the refractive index of the air. These large-scale refractive index inhomogeneities are broken up by turbulent wind and convection, spreading the scale of the inhomogeneities to smaller sizes [11].

In the case where we are imaging through a random medium, the pupil function may be split into a product of two functions, one representing the effect of the random medium, and one representing the pupil function of the imaging component;

$$H(\eta,\gamma) = A(\eta,\gamma)Z(\eta,\gamma) \qquad (5)$$

where $A(\eta,\gamma)$ is the pupil function of the imaging part of the system which is exactly the same as that given by Eq.(1) and $Z(\eta,\gamma)$ is the complex amplitude at the imaging aperture due to a point source in the object plane.

Substiting of Eq. (5) into (3) yields,

$$T(u,v) = \int_{-\infty}^{+\infty}\int_{-\infty}^{+\infty} A(\eta',\gamma')A^{\bullet}(\eta+\eta',\gamma+\gamma')\, Z(\eta',\gamma')Z^{\bullet}(\eta+\eta',\gamma+\gamma')\,d\eta'd\gamma' \qquad (6)$$

The transfer function of the random medium / imaging system for normal time- averaged imaging may be found by taking the ensemble average of $T(u,v)$. Thus,

$$\langle T(u,v)\rangle = \int_{-\infty}^{+\infty}\int_{-\infty}^{+\infty} A(\eta',\gamma')A^{\bullet}(\eta+\eta',\gamma+\gamma')\, \langle Z(\eta',\gamma')Z^{\bullet}(\eta+\eta',\gamma+\gamma')\rangle\, d\eta'd\gamma' \qquad (7)$$

The autocorrelation function of $Z(\eta,\gamma)$ is defined as:

$$C_Z(\eta,\gamma) = \langle Z(\eta',\gamma')Z^{\bullet}(\eta+\eta',\gamma+\gamma')\rangle \qquad (8)$$

The transfer function of the optical system only may be written as:

$$T_o(u,v) = \int_{-\infty}^{+\infty}\int_{-\infty}^{+\infty} A(\eta',\gamma')A^{\bullet}(\eta+\eta',\gamma+\gamma')\,d\eta'd\gamma' \qquad (9)$$

This is exactly the representation given by Eq.(3), and therefore,

$$\langle T(u,v)\rangle = T_o(u,v)C_Z(\lambda fu,\lambda fv) \qquad (10)$$

The form of $C_Z(\lambda fu,\lambda fv)$ falls to zero much faster than $T_o(u,v)$, and the resolution is therefore limited by the seeing [10].

Simulations:

Consider an extremely distant quasimonochromatic point source located on the optical axis of a simple imaging system. In the absence of atmospheric turbulence, this source would generate a plane wave normally incident on the lens. In the presence of the atmosphere, the plane wave incident on this inhomogeneous medium propagates into the medium, and ultimately a perturbed waves falls on the lens. The field distribution incident on the lens can be expressed as,

$$Z(\eta,\gamma) = e^{i\phi(\eta,\gamma)} \qquad (11)$$

where $\phi(\eta,\gamma)$ is the random phase of the incident wave front. The instantaneous psf of the entire telescope atmosphere system is given by:

$$\mathrm{psf}(x,y) = \left|FT[H(\eta,\gamma)Z(\eta,\gamma)]\right|^2 \qquad (12)$$

$H(\eta,\gamma)$ is taken to be a two dimensional circular function according to Eq.(1). The actual size of the array (M by N) is taken to be 512 by 512 pixels. This size is taken as large as possible in order to keep the theoretical diffraction limit of the telescope of interest to be truncated at zero value inside this array. In the absence of atmospheric turbulence, the phase function in Eq. (11) becomes zero and $Z(\eta,\gamma)=1$. The psf and MTF, $|T(u,v)|$, at different telescope apertures are shown in Figs. (2 and 3).

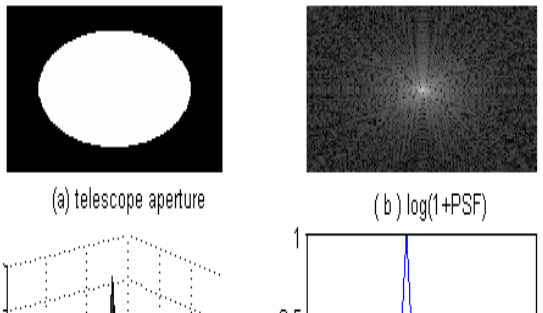

Fig.(2): ***psf and MTF as a function of telescope diameter(R=120)***

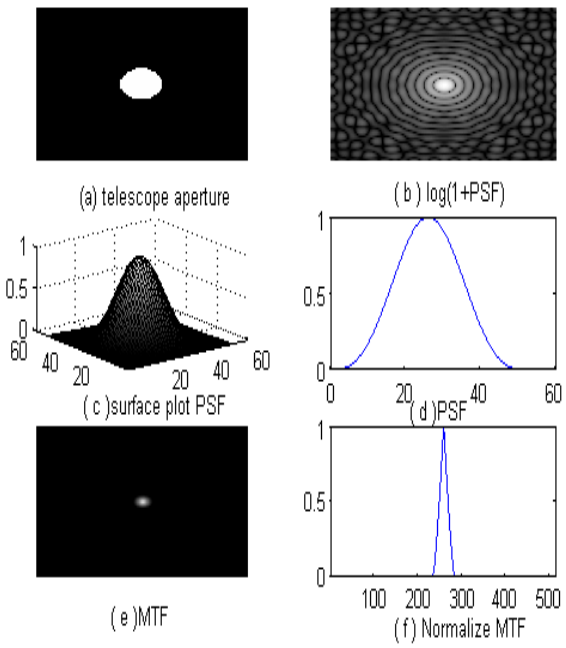

Fig.(3): ***psf and MTF as a function of telescope diameter(R=12.5).***

These two figures demonstrate that the faint details of the psf for R= 120 are much sharper then that of R=12.5. It should be pointed out here that as $R \to \infty$, the psf becomes delta function and MTF becomes nearly constant.

The MTFs at different R are normalized to one at maximum,

$$MTF_N(x,y) = \frac{MTF(x,y)}{MTF(0,0)} \qquad (13)$$

where *MTF(0,0)* represents the value of the D.C. (i.e. the central value of the array).

The average frequency components (AFC) of $MTF_N(x,y)$ is computed by:

$$AFC = \frac{1}{NM}\sum_{y=1}^{M}\sum_{x=1}^{N} MTF_N(x,y) \qquad (14)$$

Fig. (4) shows the effect of R on the actual value of AFC in the absence of atmospheric turbulence. The figure illustrates a new fact that AFC is nearly proportional to the square of the telescope radius.

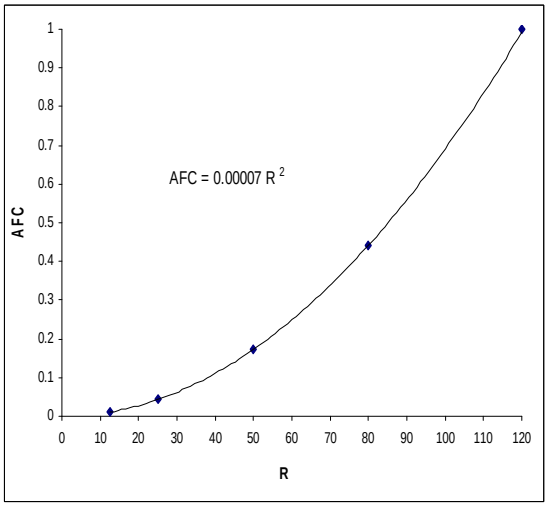

Fig. (4): ***AFC as a function of R.***

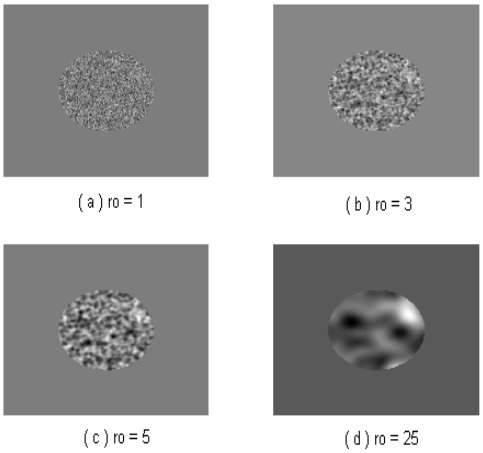

Fig. (5): ***The real parts of the complex wave front at the exit pupil for different seeing conditions (R=120).***

Now in the presence of atmospheric turbulence, $Z(\eta,\gamma)$ is taken to be a Gaussian random distribution (i.e. the real and imaginary parts are Gaussian random distribution). This function is then convolved with a normal Gaussian function (G) following the equation,

$$G(x,y)=e^{-l(x-x_c)^2+(y-y_c)^2]/(2\sigma^2)} \qquad (15)$$

where x_c and y_c represent the centers of the array and σ is the standard deviation of the Gaussian, σ is taken to be r_o which is called the Fried coherent diameter [12]. The result of this convolution is another complex function at a certain seeing condition. (i. e., $Z(\eta,\gamma)$ is a complex function at certain seeing condition r_o). The real parts of this complex wave front of an unresolved star at the exit pupil (*R=120*) for different seeing conditions are shown in Fig. (5).

The figure demonstrates very clearly, that as r_o increases the size of the spots increases and as $r_o \to \infty$, the pupil function becomes purely uniform (all the values inside the pupil becomes the same and this is the case where there is no any trace of turbulent atmosphere).

Short exposure psfs at different seeing conditions, r_o, for *R=120* are generated. Fig.(6) demonstrate the results for *R*=120. Each image represents the speckle image of an unresolved star.

To estimate the long exposure psf, either Fourier transforms of Eq. (7) is computed via generating a series of N realization of $Z(\eta,\gamma)$ and then taking the inverse Fourier transform or equivalently generating N short exposure images of psf via Eqs.(2 and 5). In this study 100 short exposure images of an unresolved star are generated and then averaged out, a Gaussian functions are then fitted to the results. Figs. (7,8,9) demonstrate this process respectively.

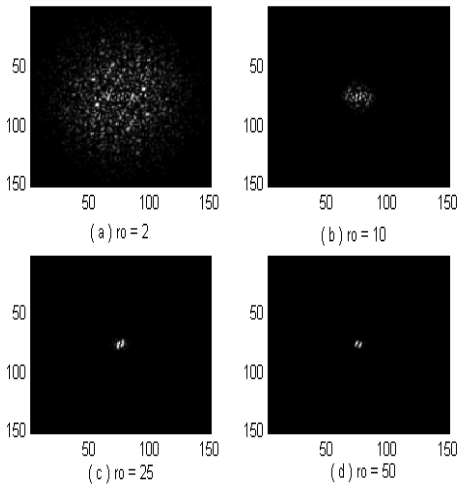

Fig. (6): ***Short exposure images of an unresolved star at different seeing condition, r_o.***

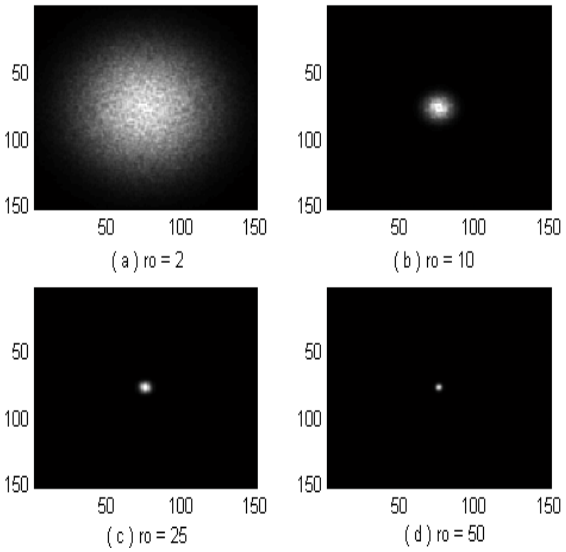

Fig.(7): ***Average psfs at different r_o (R=120).***

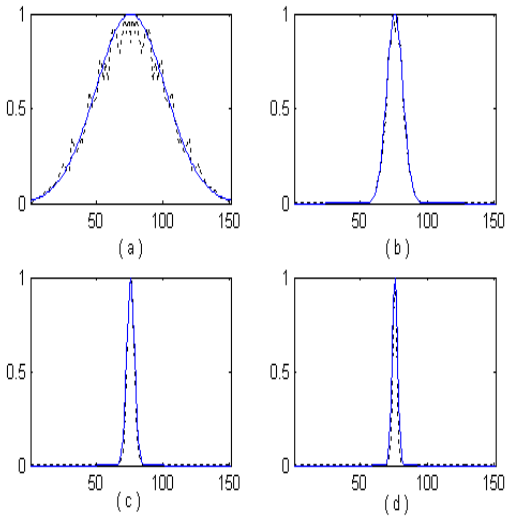

Fig.(8): ***Gaussian fitting psfs. Dotted lines representing central lines through Fig.(7).***

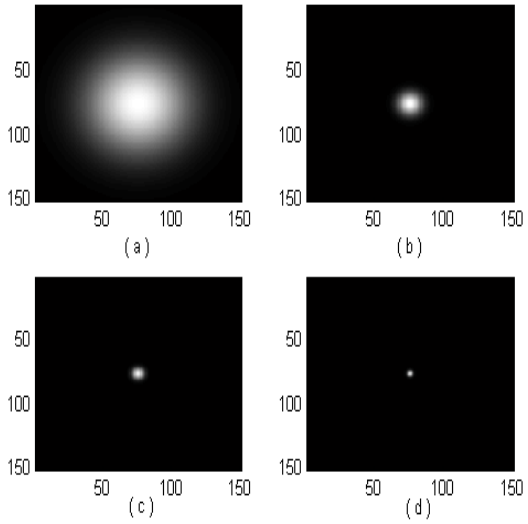

Fig. (9): ***Long exposure psfs corresponding to Fig. (7).***

To see the effect of the seeing condition, r_o, on the actual frequency components of long exposure image of an unresolved star. *AFC* is

calculated following Eq. (14). The results are shown in Figs. (10 and 11).

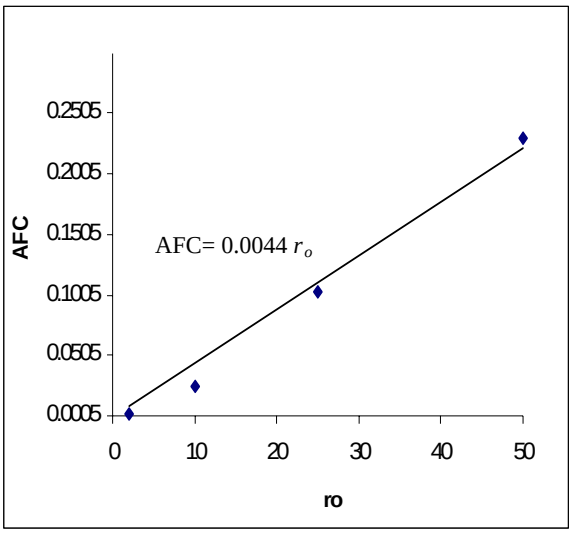

Fig. (10): ***Long exposure AFC as a function of r_o (R=120).***

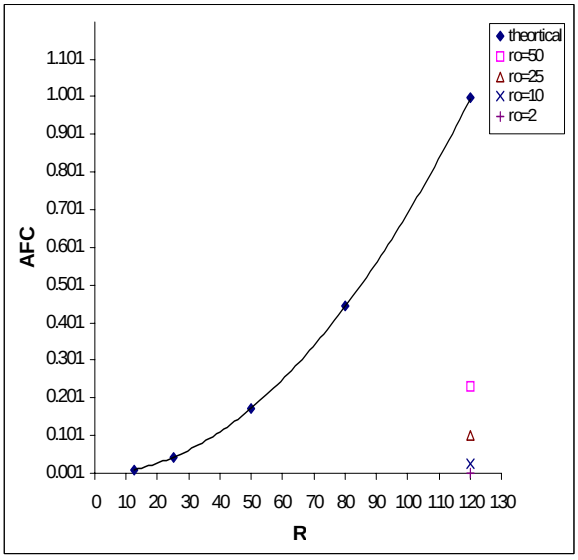

Fig. (11): ***AFC* as a function of *R*.**

Fig. (10) is also demonstrates a new fact that in the presence of atmospheric turbulence, *AFC* is linearly proportional to r_o . Fig. (11) show how the seeing conditions are severely affect *AFC* for large *R* and this will be reduced as *R* decreases.

Now, we turn our study to examine the effects of the seeing condition on actual parameters of a short exposure image of a binary star. Each speckle image as generated before is added to its a shifted version of itself to create a high light level image of a binary star, *g(x,y)*. The shift that used in all cases is (5, 5), i. e. a small shift relative to the width of the seeing disc.

The autocorrelation function of an image of binary star is then computed by:

$$C(\Delta x,\Delta y) = \int\int_{-\infty}^{+\infty} g(x,y)g(x+\Delta x, y+\Delta y)dxdy$$
$$= g(x,y) \bullet g(x,y)$$
$$= \{f(x,y) \otimes f(x,y)\} \bullet \{psf(x,y) \otimes psf(x,y)\} \qquad \textbf{(16)}$$

where $\bullet$ denotes autocorrelation.

The short exposure image of an unresolved star, binary star, power spectrum, and the autocorrelation function at different seeing conditions and at different R are shown in Figs. (12 to 20).

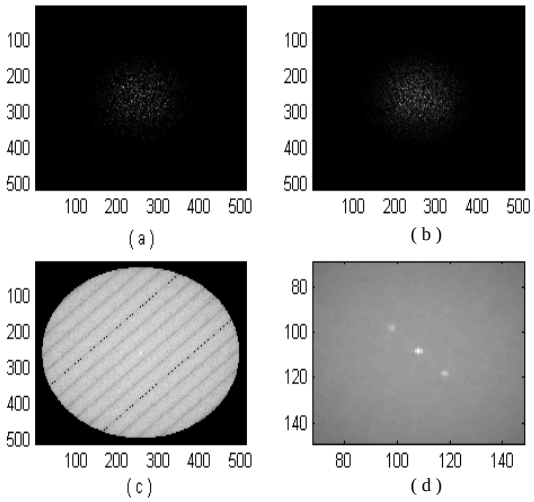

Fig. (12): ***Simulation (R=120, r_o=1)***
(a) Short exposure psf
(b) Short exposure binary star
(c) Power Spectrum
(d) Autocorrelation function

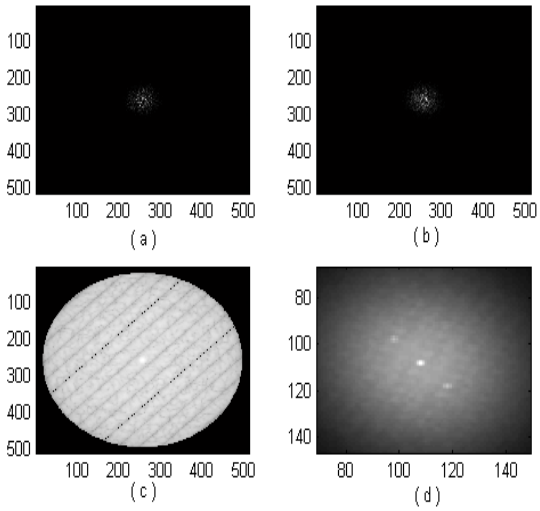

Fig.(13): ***Simulation (R=120,r_o=3)***
(a) Short exposure psf.
(b) Short exposure binary star.
(c) Power Spectrum.
(d) Autocorrelation function.

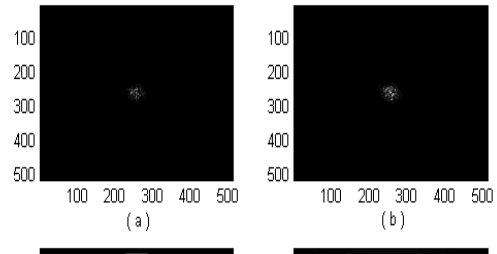

Figs.(12 to 14) demonstrate very clearly that the sharpness of the signal (R=120) remains visually unchanged as long as the seeing conditions increases (i.e., the sharpness of the signal is independent of the seeing conditions).
The same process is then repeated with R=50 pixels and the results are depicted in Figs. (15, 16, 17).

Fig.(17): ***Simulation (R=50, r_o=5)***
(a) Short exposure psf.
(b) Short exposure binary star.
(c) Power Spectrum.
(d) Autocorrelation function.

It should be pointed out here that as R decreases, the actual size of the power spectrum is also decreases. The signal becomes wider and smoothes.

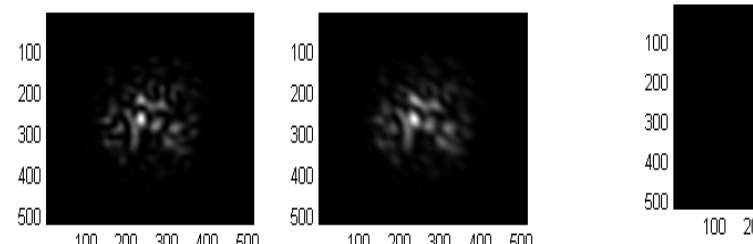

Fig. (20): ***Simulation (R=12.5,*** $r_o = 5$ ***)***

(a) Short exposure psf.
(b) Short exposure binary star.
(c) Power Spectrum.
(d) Autocorrelation function.

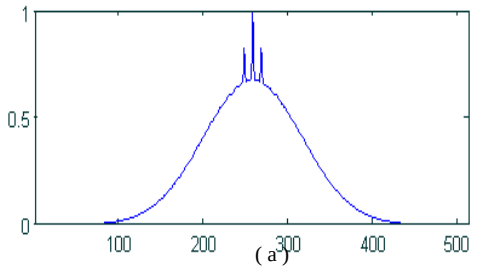

(a)

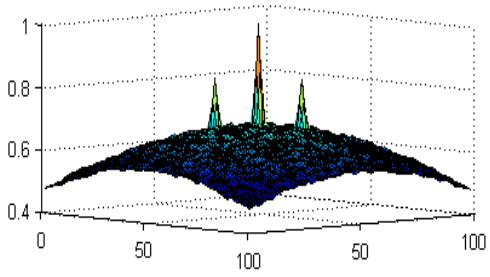

(b)

Fig. (21): ***Autocorrelation function (R=120,*** r_o ***=1)***

a- Diagonal line through Fig.(12d)
b- Perspective plot of Fig.(12d)

Figs. (18 to 20) shows that the signal is disappear. This is because the separation of a binary star is within the width of the psf of the telescope.
The diagonal lines of the autocorrelation functions and the surface plots of the preview figures are shown in Figs. (21 to 25).

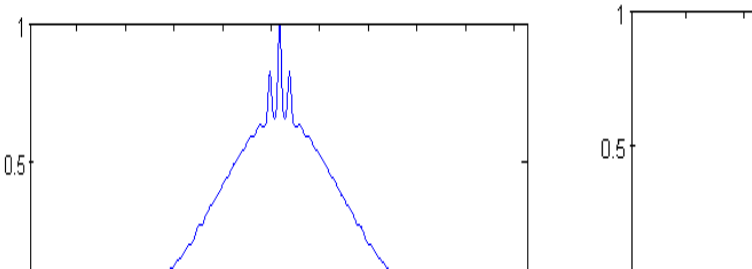

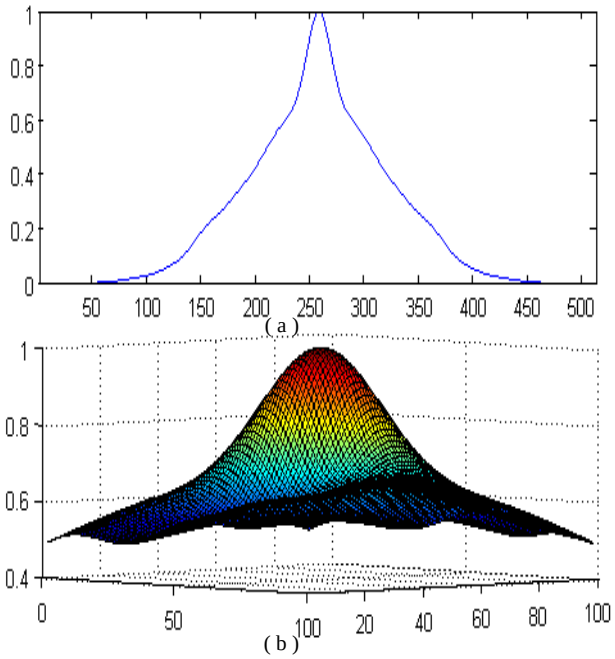

Fig. (23): ***Autocorrelation function (R=12.5, r_o =1)***
a- Diagonal line through Fig. (18d).
b- Perspective plot of Fig. (18d).

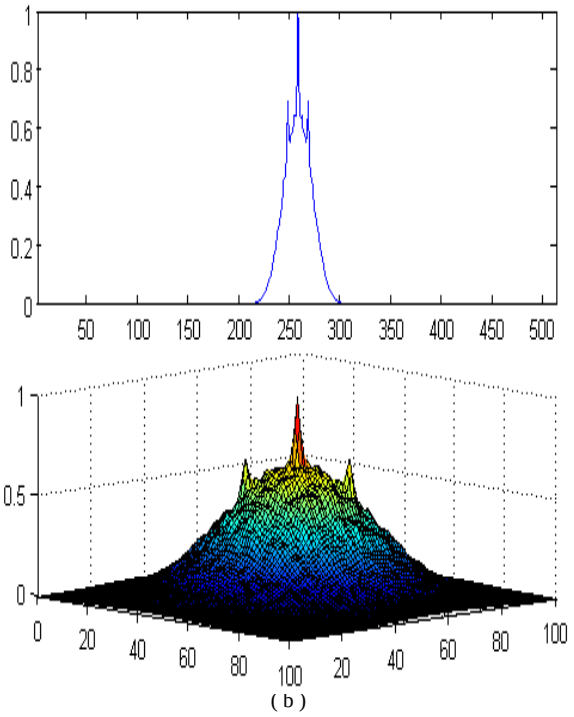

Fig. (25): ***Autocorrelation function (R=120, r_o =5)***
a- Diagonal line through Fig. (14d).
b- Perspective plot of Fig. (14d).

The signal, background, signal to background ratio, signal to noise ratio, and the width at half maximum of the autocorrelation functions are calculated for the above figures as described in Fig.(26).

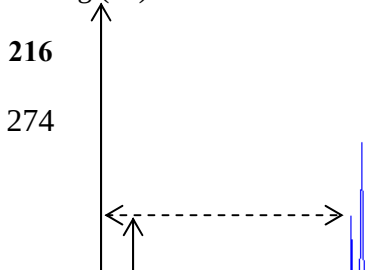

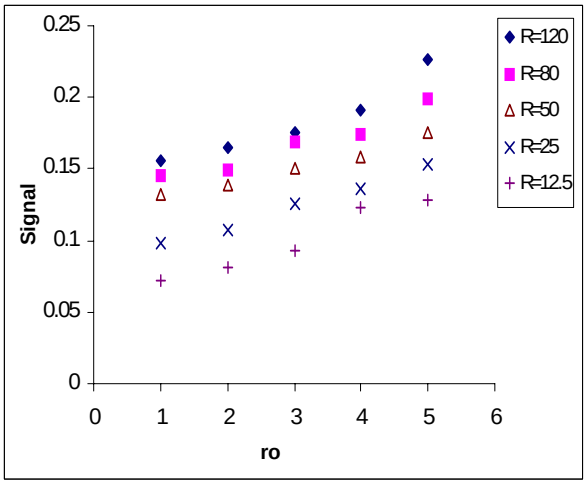

Fig. (27): ***Signal as a function of*** r_o ***for different values of R.***

The value of the secondary peak in the line autocorrelation function is taken to be the value of S+*B*, the background is calculated from the average values of the points that located at a distance $\sqrt{5^2+5^2}$ from the center of the array.

The standard deviation of the noise is estimated from the standard deviation of the values which taken for the estimated of the background.

The results of these calculations are shown in the following figures:

Fig. (28): ***Background as a function of*** r_o ***for different values***

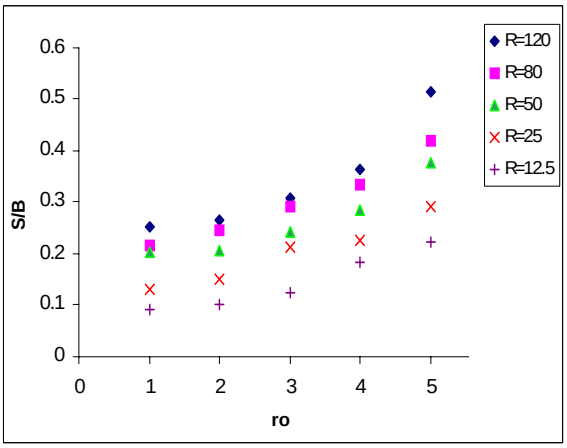

Fig. (29): ***Signal to Background ratio as a function of*** r_o ***for***

Fig. (27) demonstrates that, for a fixed telescope diameter, as the seeing condition gets better (r_o increases), the signal is also increases slightly (i.e., no significant change in signal values).

Fig. (28) shows that, for a fixed telescope diameter, as the seeing condition gets better (r_o increases), the background is decreases significantly. Therefore, the signal to background ratio is increases with increasing r_o as shown in Fig. (29).

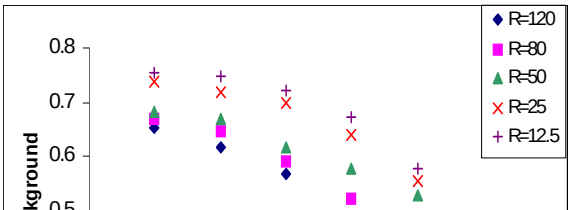

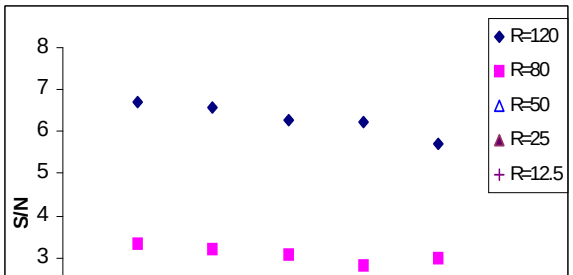

Fig.(30) shows that for larger telescope, the signal to noise ratio is slightly decreases with increasing r_o. As the telescope diameter decreases, the signal to noise ratio becomes unchanged. Fig. (31) shows that the FWHM of the autocorrelation function is decreasing exponentially as r_o increases.

Conclusions:

The following conclusions could be drawn:

1. *AFC* is found to be linearly proportional to the square of the telescope radius.
2. *AFC* is linearly proportional to the seeing conditions, r_o.
3. When the seeing condition r_o gets better and even at $r_o / R \cong 0.04$ the *AFC* is still far away from the actual value in the absence of atmospheric turbulence.
4. For large telescope, the speckle size is very small, and for $R \to \infty$, the speckle size is nearly a delta function. The secondary pea of the autocorrelation functions are also nearly delta functions.
5. For a telescope of small diameter, there is no significant change in the signal as r_o increases. As the telescope diameter increases, the signal is slightly increases.
6. As the seeing conditions increases, the background is significantly decreases. This leads to high signal to background ratio.
7. The signal to noise ratio as a function of the seeing condition is not changes significantly and is considered to be unchanged.
8. The size of the fringes of the power spectrum is linearly proportional to *R*.

References:

1. Sridharan, R., Venkatakrishnan, P., (**1999**), "*Speckle Image Reconstruction of Solar Features*", Presented at the XIX ASI meeting, Bangalore, India, Feb. 1-4.
2. Sarazin, M., and Roddier, F., (**1990**), "*The ESO Differential Image Motion Monitor*", Astron Astrophysics, 227, 294-300.
3. Ulich, B.L., and Davision, W., (**1985**), "*Seeing Measurements on Mount Graham*", Pub. Of the Astron. Soc. Of the Pacific., 97:609-615.
4. Monnier, J. D., (**2003**), "*Optical interferometry in astronomy*", Rep. Prog. Phys. 66, 789–857.
5. Fried, D.L., (**1965**), "*Statistics of a Geometric Representation of Wave front "Distortions*", JOSA Vol. 55, No. 11.
6. Kolmogorov, A. N., (**1941**), "*Dissipation of Energy in Locally Isotropic Turbulence*", Doklady Akad. Nauk SSSR 32, 16, (Translation in Turbulence, Classic Papers on Statistical Theory, eds. Friedlander, S. K. and Topper, L., Interscience, NY 1961).
7. Tatarski, V. I., (**1961**), "*Wave Propagation in a Turbulent Medium*", Translated by Silverman, R.A., McGraw-Hill Book Company, NY, NY.
8. Dainty, J.C.,Hennings, D.R., and O'Donnell, K.A., (**1981**), "*Space-Time Correlation of Stellar Speckleatterns*", J. Opt. Soc. Am., Vol. 71, p.490.
9. Welsh, B.M., and Roggemann, M.C., (**1995**), "*Signal-to-Noise Comparison of Deconvolution from Wave Front Sensing with Traditional Linear and Speckle Image Reconstruction*", Published in Applied Optics, Vol. 34, pp.2111-2119.
10. Dainty J.C., (**1973**), "*Diffraction-Limited Imaging of Stellar Objects Using*

11. Saha, S.K., (**1999**), "*Emerging Trends of Optical Interferometry in Astronomy*", Bull. Astron. Soc. India 27,441-546.
12. Fried, D.L., (**1966**), J. Opt. Soc. Am., 56,

Telescopes of Low Optical Quality ", Optics Communications, Vol. 7, No. 2.